ADVANCED FUNCTIONAL MATERIALS
www.afm-journal.de

Enhanced Field Ionization Enabled by Metal Induced Surface States on Semiconductor Nanotips

*H. Karaagac and M. Saif Islam**

Recent progress in the realization of material structures with quantum confinement and high surface to volume ratio in nanoscale interwoven metal and semiconductor building blocks offers a strong potential to build highly functional nanodevices. Ultra-sharp tips with distinct material dependent properties of metal and semiconductor exhibit important functionalities in devices including gas ionization sensors, field emission devices, and ion-mobility spectrometry. Herein, a dramatically enhanced field ionization process and a device based on charged particle beams for which the geometrical and surface properties of the constituent semiconductor nanotips are engineered with controlled introduction of metallic impurities to realize close to three orders of magnitude reduction in the ionization electric-field strength are described. Experimentally observed low voltage field ionization phenomenon is explained using the geometrical field enhancement, surface states induced by controlled introduction of metallic impurities, and polarizabilities of gas particles at the nanotips. The nanotips are employed to design field ionization gas sensors whose nanoscale pristine semiconductor tips are controllably decorated with atomic metal impurities to boost the electron tunneling properties under extremely low bias voltages. These devices also outperform their solid-state macroscopic counterparts in terms of simplicity of their construction and higher selectivity.

1. Introduction

In recent years, gas sensors have attracted a great deal of research interest due to their importance in monitoring and controlling industrial green house gas emission, indoor air quality of homes and public places, manufacturing plants, automotive emission, waste disposal and treatment plants, chemical and biochemical detection for counter-terrorism, or to diagnose medical symptoms and signs of certain diseases.[1–4] In general, gas sensors are classified into two groups based on the operating principal of the receptors: chemical and physical sensors. A chemical gas sensor is based on the change in the resistivity of the surface of an active layer upon exposure to gas molecules.[5–8] Even though most of the gas sensors are chemical in nature, they are not ideal for gas detection due to several limitations including the need for high working temperature, difficulties in detection of inert gases caused by their low adsorption energy or low electronegativity, lack of selectivity required for a gas in a complex mixture, difficulty of integrating low-cost resetting circuits for desorbing the gas molecules and high power consumption.[7] Unlike a chemical gas sensor, a physical sensor enabled by the field ionization (FI) processes is not constrained by the chemical reaction between the analyte molecules and the receptors. Recent developments have enabled physical gas sensors based on fingerprinting the ionization characteristics of different gases using one-dimensional ultra-sharp nano-materials such as nanotubes or nanowires.[9]

Conventional physical gas sensors based on gas ionization are limited by their bulky architecture, high power consumption and unsafe high-voltage operation.[10] Nanoscale materials therefore have gained much interest for the fabrication of field ionization gas sensors (FIGS) that offer crucial advantages including low cost, fast resetting, high sensitivity and high selectivity.[10] Various studies have been reported on utilizing novel nanostructures in the FIGS. Yong and co-workers reported the fabrication of a FIGS based on carbon nanotubes (CNTs) to identify CH_4-CO mixture mixed with N_2.[11] Carbon nanotubes with diameter ranging from several nanometers to several tens of nanometers have also been reported for high performance field ionization (FI) as well as field emission (FE) due to the field enhancement at their sharp tips.[10,12,13] However, although CNTs are employed for the detection of various gases, including air, He, Ar, and gas mixtures at relatively low breakdown voltages, they show poor stability under oxygen-rich ambient in which rapid degradation of the tips is triggered.[4,7,13–15] By contrast, FIGS based on metallic nanostructures such as gold (Au) nanowires (NWs) are not susceptible to oxidation, but they are relatively expensive and difficult to synthesize.[10,16–18] FIGS enabled by silicon (Si) NWs offer many advantages over CNTs and Au NWs in terms of cost, well-understood material and physical parameters, ease of processing and integration, and relatively low-voltage ionization properties.[19,20]

In the present investigation, we demonstrate FIGS with Si NWs whose nanoscale pristine tips are controllably decorated

Dr. H. Karaagac, Prof. M. Saif Islam
Northern California Nanotechnology Center and
Department of Electrical and Computer Engineering
University of California-Davis
Davis, CA, 95616, USA
E-mail: sislam@ucdavis.edu

DOI: 10.1002/adfm.201303308

© 2013 WILEY-VCH Verlag GmbH & Co. KGaA, Weinheim

with atomic metal impurities to dramatically enhance the electron tunneling properties and ionization characteristics under significantly lower ionization potential. In our device, an ensemble of pristine Si NWs synthesized via electroless etching (EE) process is configured as an anode. Among the various fabrication methods of Si NWs,[21,22] EE process is very efficient because it allows for the cost effective production of vertically aligned Si NWs for large-scale applications. Following the synthesis, the NWs were covered by a very thin layer of Au using electron-beam deposition technique to boost the density of unoccupied surface states.[23–26] We hypothesize that increased number of surface states contributes to higher probability of tunneling of valance electrons from the gas atoms or molecular potential well into these unoccupied states on Si NWs.

Schmidt and co-workers[26] have conducted a study based on the deposition of 200 nm Au onto p-Si (at substrate temperature of 78 K) to investigate the impact of unoccupied states in the band structure of the surface and the bulk. Using field-ion energy spectroscopy measurements, they observed the formation of an intermixed Si-Au region. In that study, unoccupied interface states were formed 0.8 eV above the valance band and extend up to 1.15 eV. At 0.95 eV above the valance band, the highest density of states ~10^{16} cm^{-2} eV^{-1} was observed. Although such thick Au film of 200 nm can contribute to interface states, they may completely shield the interface states and reduce their active role in the field ionization process. Compared to the bulk Si states, much higher density of unoccupied localized states was observed at the Au/p-Si surface. Salvan and co-workers reported the formation of unoccupied surface states by depositing 1 mL of Au on Si and measured significantly increased density of surface states using scanning tunneling microscopy.[23] We recently conducted a study on FIGS enabled by ultra-sharp branched Si NWs and demonstrated improved performance on ionizing Ar, N_2, He, and NH_3 under wide pressure ranges.[19,20] Other independent studies on the determination of unoccupied surface states by depositing Au on Si were reported by Freeman and Muret.[24,25]

The objective of the present study is to form both surface and bulk states through the deposition of a thin layer of Au onto pristine Si NWs based FIGS to enable enhanced FI process by expediting the tunneling of electron of specific gas particles into the unoccupied localized surface states of the NWs. The fabricated sensors have been tested for the detection of both oxygen (O_2) and ammonia (NH_3) gases, which are crucial due to their importance in many applications including environmental monitoring, control of chemical process, space missions and medical diagnostics.[2,3,27]

2. Theoretical Framework and Results

2.1. Theory of Tunneling-Field Ionization

The field ionization through electron tunneling is a process by which a neutral atom or molecule is ionized through the tunneling of their valence electron bound by a potential well into the vacuum or unoccupied states of a tip surface under high applied electric field.[28] In the context of quantum mechanics, this process is based on the assumption that the valance electron of a neutral atom is trapped in a potential well to the depth equal to the ionization potential of an atom (V_I).[29] In the presence of an external electric field (E), the probability of tunneling of an electron trapped in a well increases due to a decreased barrier height. In other words, as the strength of electric field increases, the width of the potential barrier becomes comparable to the de Broglie wavelength of the trapped electron, which subsequently gives rise to an increase in the probability of its tunneling into either vacuum or unoccupied states.[29] For a metallic surface under electric field with a gas atom in its close proximity, the probability of tunneling of an electron from the gas atom increases owing to the deformation of the potential well enabled by the Coulombic atom–metal surface interactions.[29]

The tunneling into an unoccupied surface state of a metallic tip occurs if the ground state of the valance electron bound to an atom (or ionizing particle) is located above the Fermi level (E_f) of the metallic tip. As depicted in **Figure 1**a,[20,29] this condition is satisfied only at a specific critical distance from the metal surface (x_c), which is defined by $eEx_c = (V_I\text{-}\Phi)$, where e, E, and Φ are electron charge, the applied field strength, and the work function of the metal, respectively. In order to estimate the ionization probability of an atom at x_c, the probability of tunneling of an electron from an atom (or gas particle) is multiplied by frequency of electron striking the tunneling barrier.

The ionization probability of a trapped electron and its frequency for striking the barrier under a certain electric field strength can be derived from the WKB approximation and Bohr model respectively, in the context of applying "effective" nuclear charge approximation to the atom under consideration.[30] Thus, it is possible to suggest that the FI current can be estimated by simply multiplying the ionization probability of an atom by the number of atoms in the ionization region per second. The critical distance condition for the ionization to take place essentially emerges from the lack of empty states below the Fermi level that an electron can tunnel into and the requirement that the energy level of the tunneling electron needs to line up with a vacant electronic state in the metal tips.

The FI theory has to be modified in the case of tunneling of an electron from an ionizing particle into the states of a semiconductor tip. In contrast to the metal surfaces, the field penetration into a semiconductor surfaces is allowed, leading to band bending that contributes to a degenerated region at the surface, as shown in Figure 1b. In such a case, the condition of tunneling is modified as $eEx_c = V_I\text{-}(\Phi + \Phi_p)$, where Φ_p is the additional work function induced by the band bending as a consequence of the field penetration, and is given by,

$$\Phi_p = \frac{E\lambda}{\varepsilon_r} \quad (1)$$

where λ and ε_r are penetration depth and relative permittivity of semiconductor, respectively. As shown in Equation 1, Φ_p is proportional to the penetration depth of the applied electric field. This explicitly states that more field penetration causes more band bending, which contributes to a reduction to the critical distance at which E_F and the ground state of the atomic electron coincide to trigger the FI process. Therefore, the decrease in x_c due to the band bending in semiconductors would imply

© 2013 WILEY-VCH Verlag GmbH & Co. KGaA, Weinheim
Adv. Funct. Mater. 2013,
DOI: 10.1002/adfm.201303308

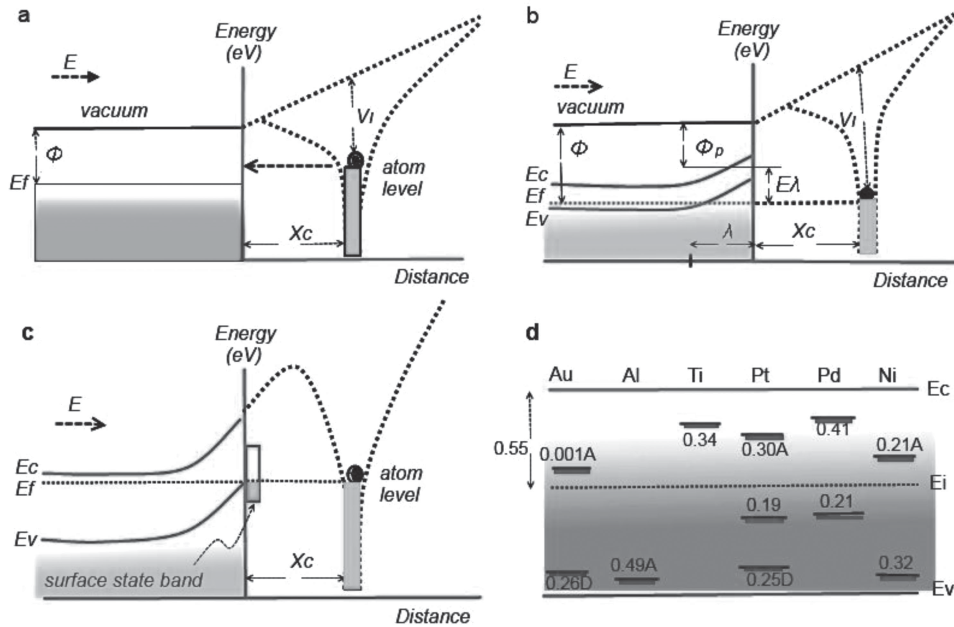

Figure 1. Energy band diagram near the surface of a metal and semiconductor, sketched based on interaction with a neutral atom, having ionization potential of V_I, located at a distance x_c (critical distance). a) The energy band structure model that shows the FI mechanism near a metal surface with work function Φ. b) Energy band diagram for a semiconductor surface. For a semiconductor with work function of Φ, the externally applied electric field (E) penetrates into the bulk up to a specific depth below the surface (λ), which subsequently results in band bending at the surface. This band bending gives rise to an increase in zero-field work function by an amount of Φ_p, which is equal to $E\lambda$. c) The effect of surface states on the energy band diagram. FI based on tunneling of valance electrons of neutral gas atoms into the unoccupied states formed at the surface. d) Position of mid-gap states caused by various metal ions added to silicon.

a higher tunneling probability and consequently an enhanced FI current with respect to a metallic surface. The incorporation of surface states via controlled introduction of metallic impurities and surface dangling bonds can form unoccupied localized states above the Fermi level, as shown in Figure 1c. These states can also contribute to the FI current by tunneling of valance electron of an ionizing atom into them.[17–20] Figure 1d shows the position of midgap states between conduction and valance bands caused by various metal ions added to silicon. Such metallic impurities can be introduced as catalysts during the bottom-up growth[20] or subsequent to the synthesis via an evaporation method.

2.2. Detection of Gases by FIGS Based on Undoped Pristine Si NWs

We characterized undoped and pristine Si NWs by fabricating sensors for detecting both NH_3 and O_2 gases. **Figure 2**a,b show the current–voltage (*I–V*) characteristics measured in the pressure range of 10^{-1}–10^{-5} Torr and a voltage range of 0–200 V for NH_3 and O_2 gases, respectively. As can be seen from the figures, in all the measured pressure ranges, devices show a typical gas discharge behavior for both gases, generally observed in the conventional planer gas sensors under uniform electric field (see Section 3 in the Supporting Information). In other words, in spite of high localized field enhancement that can be obtained through 1D nanostructures, the FI process based on quantum tunneling is not observed for the anodes designed with such pristine NWs. Factors that effect FI current include the density and aspect-ratio of NWs as well. The relationship between the density of Si NWs and FI current can be revealed by a synthesizing the Si NWs with controlled size and spacing. Understanding the role of these potential parameters is a part of our ongoing study. More discussions on the gas sensor designed with pristine NWs are presented in the Supporting Information.

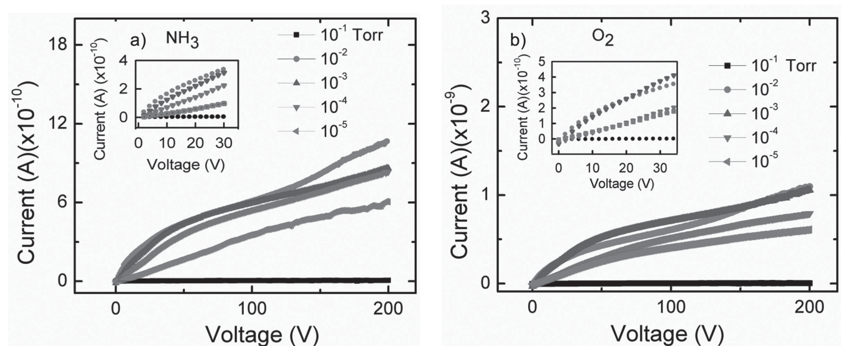

Figure 2. Current–voltage (*I–V*) characteristics of the FIGS with pristine NWs in the pressure ranges of 1×10^{-1}–1×10^{-5} Torr for a) NH_3 and b) O_2 gases. b) Inset figure shows the *I–V* curves at low voltages. The FI process is not observed with these pristine NWs even at high bias voltages.

© 2013 WILEY-VCH Verlag GmbH & Co. KGaA, Weinheim

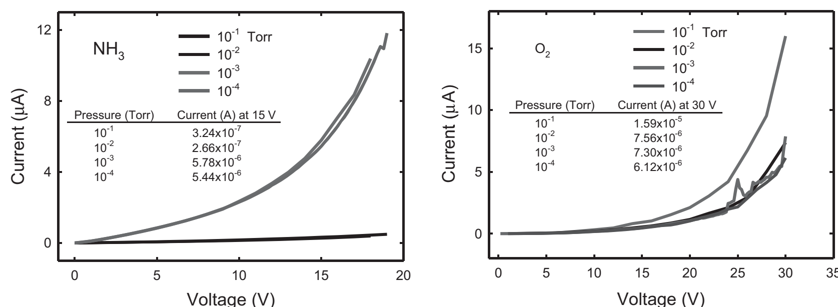

Figure 3. *I–V* characteristics of the FIGS in the pressure range of 1×10^{-1}–1×10^{-4} Torr for a) NH_3 and b) O_2 gases with Au coated Si NWs. The tables in the insets present the measured ionization currents obtained under different pressure ranges. A dramatically enhanced FI process is observed with these Au coated Si NWs (close to three orders of magnitude reduction in the ionization electric-field strength compared to that of the pristine NWs, as shown in Figure 3).

2.3. Detection of Gases by FIGS Designed with Au Coated Si NWs

The sensors based on Au coated Si NWs configured as anode have been characterized in both NH_3 and O_2 gases within pressure the range of 10^{-1}–10^{-4} Torr at room temperature. The pressure dependence *I–V* characteristics of device in NH_3 and O_2 ambient are represented in **Figure 3**. A table including ionization currents at 15 V and 30 V biases between 1×10^{-1} and 1×10^{-4} Torr pressure ranges is also presented as an inset of the figures. As shown in Figure 3a, *I–V* curves reveal two distinct regimes at all pressure levels in the voltage ranges studied. At low voltages (0–10 V), there is a nearly Ohmic region, governed by the current already generated through existing radiation-based electron-ion pairs (EIPs) between the anode (Au coated Si NWs) and the cathode (Al sheet) electrodes in the presence of an applied external electric field ($\boldsymbol{E}$). As highlighted in the Supporting Information, the current density in Ohmic region is mainly determined by concentrations and mobilities of generated EIPs and their field dependence (see Equation S1 in the Supporting Information).

As the voltage is further increased (above ≈10 V), a second distinct region appears, in which the ion current increases steeply with increasing applied voltage. In this region, the current is generated through the tunneling of electrons from the gas particles around the tip and is known as field-limited regime, in which the current (I) can be expressed by Gomer's relation,[31] $I = 2\ \pi r_t^2 q\ x_c c_t \nu_e D$, where r_t, c_t, ν_e, and D are tip curvature, gas concentration near the tip, orbital frequency of the tunneling electron and tunneling probability, respectively. To contrast the Ohmic and field-limited regimes, the *I–V* characteristic of a sensor tested in NH_3 at a pressure of 10^{-4} Torr is re-drawn in **Figure 4**a in linear scale with an inset showing current versus electric field variation. Figure 4b shows *I–V* characteristics in log-log scale. It is important to note that at low voltages between 0–10 V (or 0–0.12 V μm^{-1}), the conduction is determined by transport of already existed radiation-generated EIPs to the counter electrodes under the applied electric field. On the other hand, with further increase in voltage (>10 V or >0.12 V μm^{-1}), it is seen that a current based on tunneling ionization is taking place within the 10–26 V range just before reaching the breakdown voltage (V_b). A similar trend is observed in the case of detection of O_2 given in Figure 4d. For metal tips, high electric field strengths are required in order to observe FI of neutral atom or molecules based on quantum tunneling. It is well-known that for most of the known gases, the required field strengths for the field ionization vary between 2 and 5 V Å^{-1}.[31] On the other hand, sensors based on semiconductor tips can reduce these threshold voltages due to existence of the field penetration in semiconductors as opposed to metals. In other words, as mentioned earlier, unlike the metal tips, a field penetration occurs on subjection of a semiconductor material to an external electric field. Field penetration, subsequently, causes band bending at semiconductor-vacuum interface by which a degenerated region consisting of unoccupied valance band states is formed to facilitate the tunneling process of valance electron of imaging gas atoms into them.[32] In semiconductors, it is also possible to introduce unoccupied local surface states through coating of a semiconductor surface with very thin layer of different metals.[23–26] The tunneling of valance electron of target gas atoms or molecules into these vacant surface states results in an increase in the field ionization current.

As discussed earlier, based on the considerations of reported studies on introducing surface states to silicon by deposition of a thin layer of Au,[23–26,33] our NWs also experienced the formation of similar states at the surfaces subsequent to the coating of 3 nm Au layer. Therefore, the observed low-threshold (10 V or 0.12 V μm^{-1}) field ionization, for example, in the detection of NH_3 can be attributed to incorporation of Au-originated vacant surface states as well as the geometrical field enhancement generated by integrated Si NWs (see Figure S4 in the Supporting Information). Given the high density of ultra-sharp NWs on our anodes (as shown in Figure 1d), it is likely that the quantum tunneling process on a large majority of the NWs is affected by the close proximity of the neighboring NWs, which is known as the "field screen effect", and a relatively small number of NWs on the edges of the substrate contribute to the high current. This may lead to poor stability over time. Our ongoing study will focus on correlating the inter NW spacing and resulting ionization currents.

When Si NWs were decorated with a thin aluminum (Al) film of 3 nm thickness, field ionization based on quantum tunneling was not observed. This is because Al contributes to deep acceptor level –0.493 eV below the Fermi level of Si, as shown in Figure 1d. By contrast, Si donor levels are only 0.27 eV above the Fermi level. Details of the measurements and discussions are presented in Figure S5 in Supporting Information, Section 4. We also conducted X-ray photoelectron spectroscopy (XPS) measurements to confirm the incorporation of Au into SiNWs. The recorded XPS survey spectra are shown in **Figure 5**a. The shift in binding energy of photoelectron lines appeared in XPS spectra was originated from surface charging effect, which was corrected based on the well-known reference binding energy of C 1s photoelectron line (284.6) as shown in Figure 5b. As

© 2013 WILEY-VCH Verlag GmbH & Co. KGaA, Weinheim
Adv. Funct. Mater. **2013**,
DOI: 10.1002/adfm.201303308

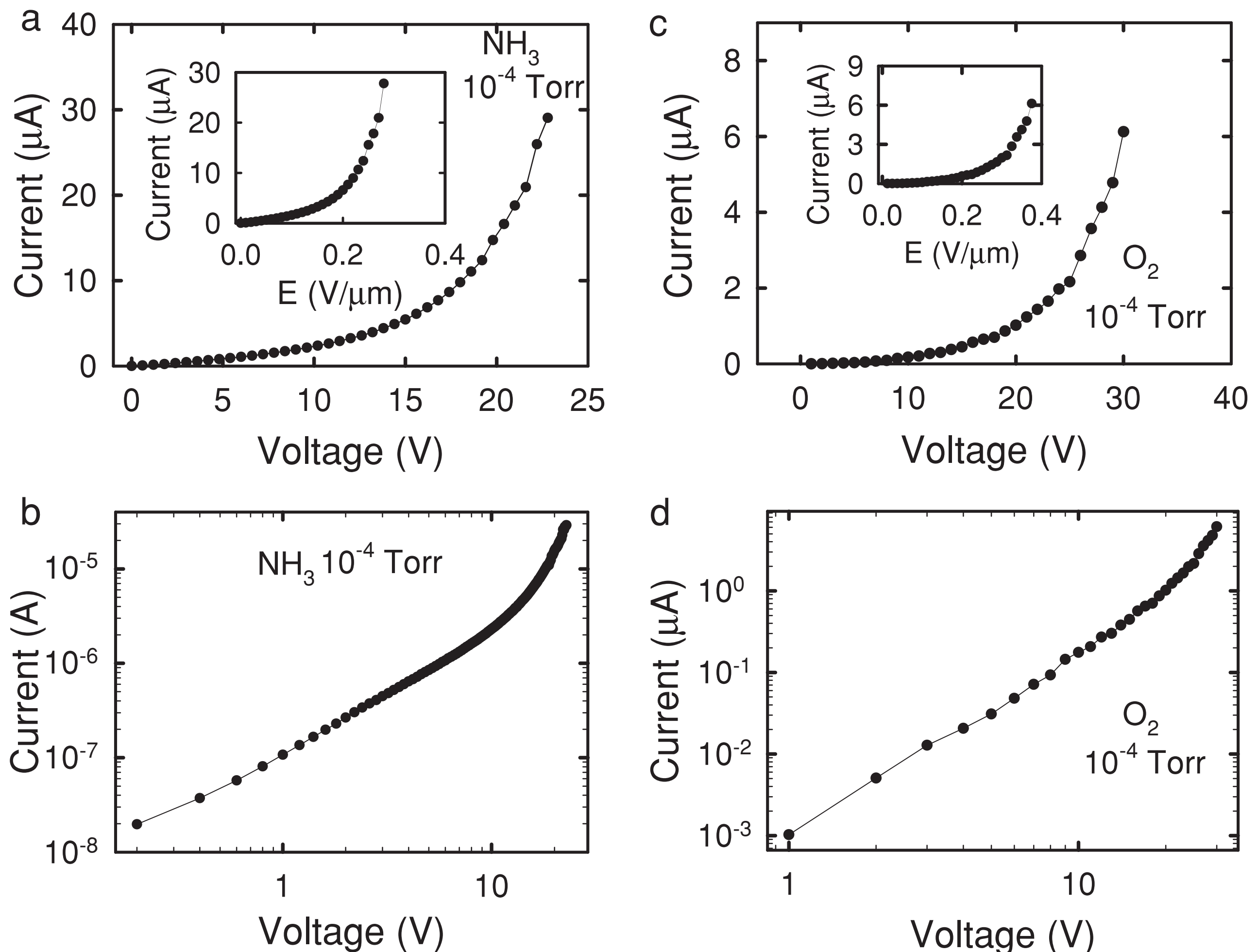

Figure 4. a) The *I–V* characteristics in linear scale under gas pressure of 1×10^{-4} Torr for NH_3. The inset shows the current variation as a function of applied electric field in linear scale for the same gas pressure. b) The *I–V* variation in log-log scale reveals both Ohmic and field-limited regions. c) The *I–V* characteristics in linear scale under gas pressure of 1×10^{-4} Torr for O_2. The inset figure shows the current variation as a function of applied electric field in linear scale for the same gas pressure. d) The *I–V* variation in log-log scale reveals both Ohmic and field-limited regions in the detection of O_2, defined for a typical field ionization gas sensor.

can be seen in **Figure 6**a, the expected elements (Au and Si) appeared in XPS survey spectra, verifying the incorporation of Au following the doping process. Besides these, carbon (C) and oxygen (O) photoelectron lines are observed. These elements got incorporated as a result of exposure to the atmosphere before the measurement or during the sample preparation. To remove the contaminated layer, the surface of Si NWs was sputtered with high energetic argon (Ar) ions (between 0.5 and 3 keV) followed by 6 different sputter-etching cycles with different time durations (between 2 and 4 min), as shown in Figure 5a. As seen in Figure 6c, following this process, there is a substantial decrease in concentrations of C and O. On the other hand, a systematic increase in those of Au and Si observed when the energy and time duration of sputtering cycle increases from 1 to 6. The evaluation of Au 4f photoelectron peak is shown in Figure 5d. It appears as doublet consisting of 4f 7/2 and 4f 5/2 resulting from the spin-orbit interaction. To identify the constructed bonds based on Au element, the shift in binding energy of constituent peaks of doublet (4f 7/2 and 4f 5/2) can be used. It is clear from the table given as an inset in Figure 5d that there is a shift in binding energy of both peaks with respect to binding energy known for the Au–Au bond, and the shift exactly matches the value known for the Au–Si bonds. The results extracted from the XPS study proves the formation of Au–Si intermixed layer following the doping process as depicted in Figure S4 of Supporting Information, Section 3.

As shown in Figure 3a, there is a decrease in current in the field-limited regime with increase in gas pressure of NH_3 at 15 V. The measured currents were 3.24×10^{-7} A and 5.44×10^{-6} A for 10^{-1} Torr and 10^{-4} Torr, respectively. Based on the Gomer's relation, the current is expected to increase with the increase in gas concentration around the tip. However, the gas concentration around the tip (ionization zone) may not be the same as it is in the region far from the tip for a specific vacuum chamber pressure (P). In other words, the gas concentration in field ionization zone determines the field ionization current and may not

© 2013 WILEY-VCH Verlag GmbH & Co. KGaA, Weinheim

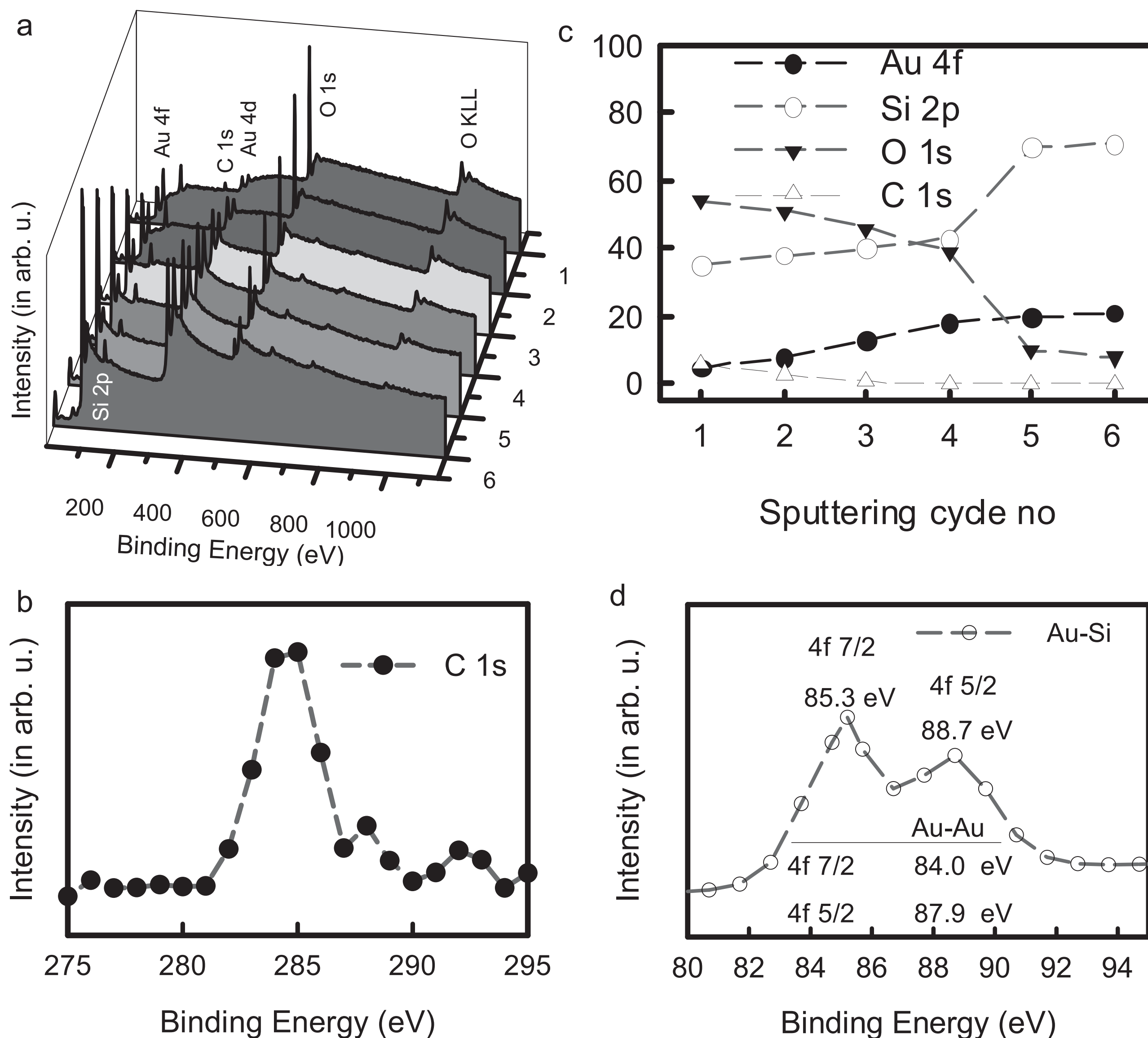

Figure 5. XPS spectra of Si NWs decorated with a thin layer of gold. a) Survey spectra after doping following 6 sputter-etch cycles carried out by using Ar ions with different energies for various etch times: 1) 0.5 keV (2 min), 2) 0.5 keV (4 min), 3) 0.5 keV (6 min), 4) 1 keV (2 min), 5) 2 keV (4 min), and 6) 3 keV (4 min). b) C 1s photoelectron line used as reference binding energy (284.6 eV) to correct surface charging effect. c) The observed change in atomic concentrations of Au, Si, C, and O in the Au/Si intermixed layer following the employed 6 sputter-etch cycles (1–6). d) XPS Au 4f photoelectron doublet appeared in spectrum following the sputtering Si NWs surface with energetic Ar ions (3 keV) for 4 min time duration. Inset table gives the well-known binding energies of 4f 7/2 and 4f 5/2 for metallic Au–Au bond. The experimentally observed binding energies for the constituent peaks of 4f doublet are found to be larger than Au–Au metallic bond, verifying the construction of Au–Si bonds in the Au/Si intermixed layer formed following the doping and annealing processes.

follow the pressure change in vacuum chamber.[18] However, it is reasonable to suggest that there would be a competition between the gas concentration in region far from the tip and the mean free path *(L)* of gas atom or molecules on determining the current-voltage behavior under a specific pressure. These are two main parameters that have a direct effect on the transportation of neutral gas atom or molecules from the far zones to the zones near the tip (onset of this region is determined by x_c) in which tunneling can take place. Therefore, the observed increase in ionization current with decrease of pressure for NH_3 may suggest that the mean free path wins this competition and dictates the variation of current with pressure. In other words, at lower pressures, there would be fewer collisions between gas particles and the arrival of increased number of gas particle positively contributes to the ionization region from which particles are ionized through the tunneling of valance electrons into vacant states of tip introduced by Au atoms. It is noticeable from Figure 3b, contrary to the variation observed in the case of NH_3, the change of pressure in the region near the tips follows the pressure change in zone far from it, indicating the dominance of P parameter over the L in terms of determination of ion current behavior for O_2 ionization.

© 2013 WILEY-VCH Verlag GmbH & Co. KGaA, Weinheim

DOI: 10.1002/adfm.201303308

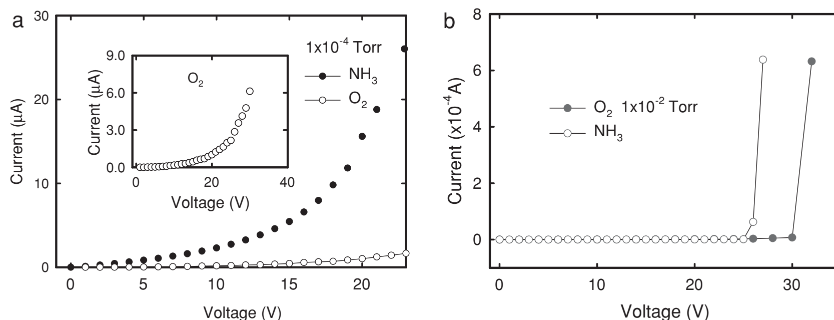

Figure 6. Detection of target gases. a) *I–V* characteristics of NH_3 and O_2 gases in the pressure of 1×10^{-4} Torr. Inset figure clearly presents the magnitude of current for O_2 under the same pressure. b) *I–V* characteristics of NH_3 and O_2 gases during the breakdown course with a pressure of 10^{-2} Torr, showing that the breakdown occurs at different voltages, namely 26 V and 32 V for NH_3 and O_2, respectively. It can be seen that the current rapidly reach very high value (≈0.65 mA) for both gases following the breakdown mechanism.

Figure 6a shows the onset of field ionization for O_2, 15 V (or 0.19 V μm^{-1}), which is higher than that obtained for NH_3, 10 V (0.12 V μm^{-1}). Interestingly, the onset of FI is unique to each individual gas and shows a close correlation to the relative ionization potential of NH_3 and O_2 gases, which are 10.15 eV and 12.06 eV, respectively.[9] Beside the ionization potential, there are also other potential factors that can determine the FI current such as polarizability of the gas particles under consideration, which is defined as the measure of the change in an atom or molecule's electron distribution in the presence of an external electric field. For highly polarizable gas particles, more supply of gas particles to the ionization zone is expected as a consequence of the increase in the probability of trapping particles in the region around the tip in which particles have high probability of being ionized through electron tunneling.

As suggested by the Gomer's relation, current in field-limited regime is dependent on the equilibrium gas concentration in the zone around the tip (c_t), which is given by

$$c_t = c_g \sqrt{\frac{T_g}{T_t}} \exp\left(\frac{U_p}{K_B T_g}\right) \quad (2)$$

where c_g, c_t, and T_t are the gas concentration far from the ionization region, gas and tip temperatures, respectively. In addition, U_p represents the polarization energy of the gas particle and is defined by

$$U_p = \frac{1}{2}\alpha_p E^2 \quad (3)$$

where α_p and E are atomic or molecular polarizability and applied electric field, respectively.[18,31,34] Equation 3 suggests that polarization potential energy plays a significant role in the concentration of gas near the tips. FI current, therefore, is expected to be improved for highly polarizable atoms or molecules. The experimental values for polarizabilities of NH_3 and O_2 gases were reported as 2.103 (Å^3) and 1.562 (Å^3), respectively.[35] As the polarizability of NH_3 molecules is higher than that of O_2, it is expected that NH_3 molecules will be more easily drawn to the Si NW tips compared to O_2 molecules, which results in more supply of electrons to the conduction for NH_3 gas through the tunneling of valance electron from these molecules into the unoccupied states in the Si NW tips. Therefore, in comparison to current measured for O_2, the obtained higher current for NH_3 under same conditions is quite reasonable based on the difference between their ionization potential and polarizabilities. As shown in Figure 6b, with further increase in the applied bias voltage, the breakdown is initiated following the field-limited regimes by exhibiting distinct breakdown voltages, namely at 26 V and 32 V for NH_3 and O_2 gases, respectively. The observed breakdown process may be triggered due to the generation of positive corona surrounding tip that leads to filling the gap between electrodes through the formation of plasma streamers.[18] Based on their ionization potentials, the higher breakdown voltage of O_2 is expected because of its higher ionization potential compared to that of NH_3. This shows that Au coated Si NWs configured as anode in a gas sensor can be used to distinguish NH_3 and O_2 gases at considerably reduced voltages. In other words, the observed different breakdown voltages associated with different gases clearly demonstrate the fingerprinting capability of the fabricated gas ionization sensor.

3. Conclusions

We demonstrated dramatically enhanced field ionization on gold coated ultra-sharp silicon nanowires and explained our observations on the basis of combination effects of geometrical field enhancement, surface states induced by controlled introduction of metallic impurities and polarizabilities of gas particles at the silicon nanotips. In some recently developed synthesis of semiconductor nanostructures, metal catalysts are used to ensure growth, orientation and their size control.[36,37] The process introduces unintentional incorporation of metal impurities in nanostructures.[38] In most cases, these catalysts adversely affect the material properties and impede the development of high-performance electronic and photonic devices. This is why in conventional electronic and photonic circuitry; metals and semiconductors serve different functions that can be traced to their distinct material-dependent properties. They are kept separated from each other in most cases except for forming Ohmic or Schottky contacts and metal interconnects to the semiconductor devices. However, catalysts enabled synthesis processes offer wide varieties of nanostructures with unmatched dimensions to enable numerous new applications and this work shows one important application of such materials. We demonstrated that pristine NWs with controlled introduction of metallic impurities offer unique advantage for FI applications due to high density of surface states associated with the impurities. Our results indicate that although unintentional incorporation of impurities in nanowires from the catalysts is detrimental to the electrical and optical properties of devices, such catalyst assisted bottom-up growth are very attractive for FI enabled applications. The FI gas sensors demonstrated here capitalize on

© 2013 WILEY-VCH Verlag GmbH & Co. KGaA, Weinheim

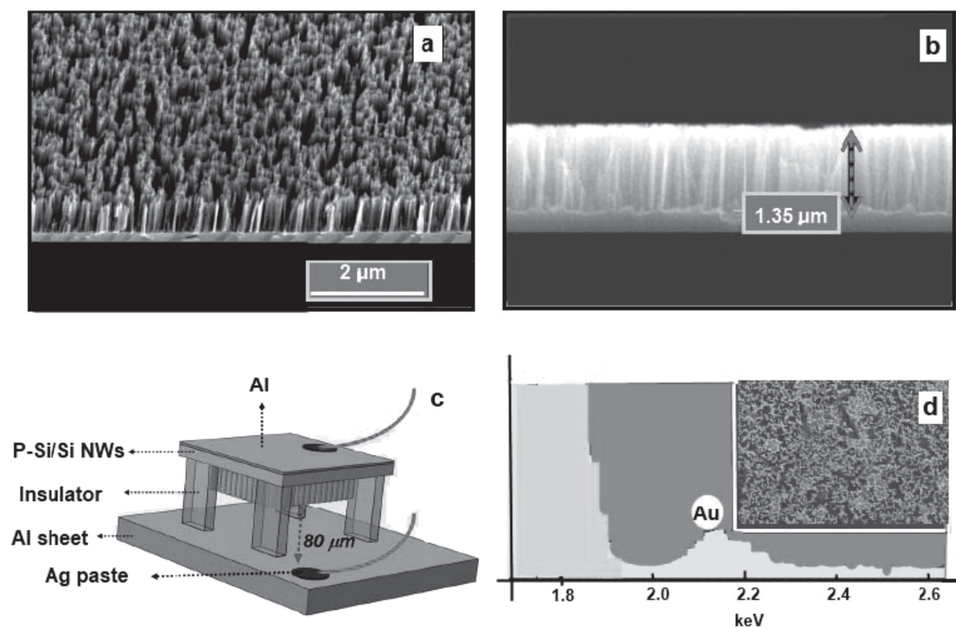

Figure 7. Scanning electron microscopy (SEM) images of the fabricated Si NWs and constructed field ionization gas sensor. a,b) SEM images of the top and cross-sectional views of Si NWs. c) Schematic representation of our gas sensor. An ensemble of Si NWs and an Al sheet serve as anode and cathode, respectively. Electrodes are separated by an 80 µm thick insulating film (separator). d) Energy dispersive X-ray analysis (EDS) spectrum verifying the incorporation of Au following the decoration of Si NWs with a thin layer (3 nm) of gold. Inset figure shows the scanned area during the measurement.

the notion that conventional catalyst assisted processes used for synthesizing semiconductor nanostructures offer great potential to rationally tailor material properties in a myriad of useful ways. Sensing devices designed using our scheme are compact, safe to use due to low voltage operation, CMOS compatible and are capable of fingerprinting a broad range of analytes with good selectivity.

4. Experimental Section

As shown in Figure 7a,b, Si NWs were synthesized on p-Si (100) substrate through Ag-assisted electroless etching (EE) technique. A pre-cleaned Si-wafer was immersed into a solution consisting of hydrofluoric acid (HF) and silver nitrate ($AgNO_3$) with concentration of 4.6 M and 0.002 M, respectively. The detailed procedure for the production of Si NWs by EE technique is reported in the literature.[28,39] During the growth cycle, the temperature and etching time were selected as 60 °C and 10 min, respectively. Previous results have shown that the density and the size of produced Si NWs are closely related to the density of metallic (Ag) particles on Si surface.[40] As is depicted in the plane and cross-sectional view in Figure 7a,b, the etched layer consist of well-aligned NWs formed perpendicular to the substrate surface with an etching depth of 1.35 µm corresponding to the average length of the NWs. In the construction of the FIGS, an ensemble of such NWs was used as an anode. NWs with different lengths can also be fabricated and employed in the construction of sensor structure by tuning the processing time, etchant concentration and the solution temperature during the etching process.[39] Moreover, patterned Si micro/nano-structures can be fabricated from the pre-patterned Ag film onto Si wafer by using electroless etching technique (see Supporting Information, Figure S1).

Following the synthesis of the NWs, they were covered by a 3 nm thin Au layer using an electron-beam evaporator at a constant rate of 3 Å s^{-1} without heating the substrate. Subsequently, the sample was annealed at 550 °C for 30 min under the N_2 gas flow. Figure 7c shows the schematic diagram of Si NW-based FIGS. Two sets of FIGS were constructed with undoped Si NWs at the anode. In one set, pristine NWs were used in the anode while in the other set, a thin Au film was delineated on the NWs and annealed. The incorporation of Au was verified through the energy dispersive X-ray analysis (EDS) spectrum shown in Figure 7d. As depicted in the Figure 7c, an Al sheet is configured as the cathode which is at 80 µm distance from the NW coated anode and is separated by a thick insulating film (separator). The effective area of the fabricated FIGS is 1 cm^2. The characterization of the devices for the detection of various gases was carried out in a custom made vacuum chamber integrated with electrical feedthroughs and mass flow controllers (MFCs). Details of the measurement system and procedure are presented in the Supporting Information. Prior to each test, the vacuum chamber was pumped down to 10^{-7} Torr and then target gases were introduced in a controlled fashion through the integrated MFCs. For the *I–V* measurement, a semiconductor parameter analyzer, two source measure units connected in series, were used and controlled by a computer. To prevent the possible charging current that can emerge from the device capacitance, the sweeping mode of voltage was chosen as staircase.

Supporting Information

Supporting Information is available from the Wiley Online Library or from the author.

Acknowledgements

This work was supported by Turkish Scientific Research Council (TUBITAK) under BIDEB-2219 program, a University of California CITRIS

© 2013 WILEY-VCH Verlag GmbH & Co. KGaA, Weinheim

DOI: 10.1002/adfm.201303308

(The Center for Information Technology Research in the Interest of Society) grant and NSF grant # CMMI-1235592.

Received: September 25, 2013
Revised: October 27, 2013
Published online:

[1] G. Hui, L. Wu, M. Pan, Y. Chen, T. Li, X. Zhang, *Meas. Sci. Technol.* **2006**, *17*, 2799.
[2] J. Kong, N. R. Franklin, C. W. Zhou, M. G. Chapline, S. Peng, K. J. Cho, H. J. Dai, *Science* **2000**, *287*, 622.
[3] Special Issue on Gas Sensing Materials, *MRS Bull.* **1999**, *18*, 24.
[4] H. Wang, C. Zou, C. Tian, L. Zhou, Z. Wang, D. Fu, *Nanoscale Res. Lett.* **2011**, *6*, 534.
[5] L. Liao, H. B. Lu, J. C. Li, H. He, D. F. Wang, D. J. Fu, C. Liu, W. F. Zhang, *J. Phys. Chem. C* **2007**, *111*, 1900.
[6] L. Liao, H. B. Lu, J. C. Li, C. Liu, D. J. Fu, Y. L. Liu, *Appl. Phys. Lett.* **2007**, *91*, 173110.
[7] L. Liao, H. B. Lu, M. Shuai, J. C. Li, Y. L. Liu, C. Liu, Z. X. Shen, T. Yu, *Nanotechnology* **2008**, *19*, 175501.
[8] Q. Wan, Q. H. Li, Y. J. Chen, T. H. Wang, X. L. He, J. P. Li, C. L. Lin, *Appl, Phys. Lett.* **2004**, *84*, 3654.
[9] J. R. Huang, J. H. Wang, C. P. Gu, K. Yu, F. L. Meng, J. H. Liu, *Sens. Actuators, A* **2009**, *150*, 218.
[10] F. L. Meng, M. Q. Li, Y. Chen, Y. Jia, J. Y. Liu, J. R. Huang, J. H. Liu, *IEEE Sens. J.* **2009**, *9*, 435.
[11] Z. Yong, L. Junhua, L. Xin, T. Xiaojun, Z. Changchun, *Sens. Actuators, A* **2005**, *125*, 15.
[12] D. Tasis, N. Tagmatarchis, A. Bianco, M. Prato, *Chem. Rev.* **2006**, *106*, 1105.
[13] M. S. Wang, L. M. Peng, J. Y. Wang, Q. Chen, *J. Phys. Chem. B* **2004**, *109*, 110.
[14] A. Modi, N. Koratkar, E. Lass, B. Wei, P. M. Ajayan, *Nature* **2003**, *424*, 171.
[15] D. J. Riley, M. Mann, D. A. MacLaren, P. C. Dastoor, W. Allison, K. B. K. Teo, G. A. J. Amaratunga, W. Milne, *Nano Lett.* **2003**, *3*, 1455.
[16] S. Kim, *Sensors* **2006**, *6*, 503.
[17] R. B. Sadeghian, M. Kahrizi, *Sens. Actuators, A* **2007**, *137*, 248.
[18] R. B. Sadeghian, M. Kahrizi, *IEEE Sens. J* **2008**, *8*, 161.
[19] R. Banan-Sadeghian, M. S. Islam, *Proc. SPIE* **2010**, *7679*, 76791D.
[20] R. B. Sadeghian, M. S. Islam, *Nat. Mater.* **2011**, *10*, 135.
[21] Y. Q. Fu, A. Colli, A. Fasoli, J. K. Luo, A. J. Flewitt, A. C. Ferrari, W. I. Milne, *J. Vac. Sci. Technol. B* **2009**, *27*, 1520.
[22] K. Peng, Y. Wu, H. Fang, X. Zhong, Y. Xu, J. Zhu, *Angew. Chem. Int. Ed.* **2005**, *44*, 2737.
[23] H. F. F. Salvan, A. Baratoff, G. Binnig, *Surf. Sci.* **1985**, *162*, 634.
[24] L. B. Freeman, W. E. Dahlke, *Solid-State Electron.* **1970**, *13*, 1483.
[25] P. Muret, A. Deneuville, *J. Appl. Phys.* **1982**, *53*, 6289.
[26] W. A. Schmidt, A. J. Melmed, M. F. Lovisa, M. Naschitzi, J. H. Block, *Surf. Sci.* **1988**, *194*, 127.
[27] Y. Takao, K. Miyazaki, Y. Shimizu, M. Egashira, *J. Electrochem. Soc.* **1994**, *141*, 1028.
[28] B. H. C. Niu, J. R. Beacham, P. J. Bryant, *J. Chem. Phys.* **1977**, *67*, 2039.
[29] J. A. Panitz, *J. Phys. E. Sci. Instrum.* **1982**, *15*, 1281.
[30] E. W. Müller, T. T. Tsong, *Field ion microscopy; principles and applications*, American Elsevier Pub. Co., New York **1969**.
[31] R. Gomer, *Field emission and field ionization*, Harvard University Press, Cambridge, **1961**.
[32] A. C. M. K. Miller, M. G. Hetherington, G. D. W. Smith, *Atom Probe Field Ion Microscopy*, Oxford, New York **1996**.
[33] S. M. Sze, *Cc/Eng Tech. Appl. Sci.* **1982**, *27*, 28.
[34] X. Liu, J. Orloff, *J. Vac. Sci. Technol., B* **2005**, *23*, 2816.
[35] NIST (National Institute of Standards and Technology)
[36] A. R. Tao, S. Habas, P. D. Yang, *Small* **2008**, *4*, 310.
[37] Y. Y. Wu, P. D. Yang, *J. Am. Chem. Soc.* **2001**, *123*, 3165.
[38] J. E. Allen, E. R. Hemesath, D. E. Perea, J. L. Lensch-Falk, Z. Y. Li, F. Yin, M. H. Gass, P. Wang, A. L. Bleloch, R. E. Palmer, L. J. Lauhon, *Nat. Nanotechnol.* **2008**, *3*, 168.
[39] B. Ozdemir, M. Kulakci, R. Turan, H. E. Unalan, *Nanotechnology* **2011**, *22*, 155606.
[40] K. Q. Peng, J. J. Hu, Y. J. Yan, Y. Wu, H. Fang, Y. Xu, S. T. Lee, J. Zhu, *Adv. Funct. Mater.* **2006**, *16*, 387.

© 2013 WILEY-VCH Verlag GmbH & Co. KGaA, Weinheim

Copyright WILEY-VCH Verlag GmbH & Co. KGaA, 69469 Weinheim, Germany, 2013.

ADVANCED FUNCTIONAL MATERIALS

Supporting Information

for *Adv. Funct. Mater.*, DOI: 10.1002/adfm.201303308

Enhanced Field Ionization Enabled by Metal Induced Surface States on Semiconductor Nanotips

*H. Karaagac and M. Saif Islam**

Supporting Information

for *Adv. Funct. Mater.*, DOI: 10.1002/adfm.201303308

Enhanced Field Ionization Enabled by Metal Induced Surface States on Semiconductor Nanotips

By *H. Karaagac* and *M. Saif Islam**

1. Details of the measurement system: Following the ohmic contacts to the electrodes, the fabricated gas sensor was placed in a custom made vacuum chamber (accommodating target gases and gas mixtures between 10^{-7} and 760 Torr) with electrical/mechanical feedthroughs and mass flow controllers (MFCs) to release the target gases into the vacuum chamber in a controlled fashion. The integrated MFCs are capable of regulating gas flow rate to 1 sccm. Pumping down of the vacuum chamber was carried out through roughing and turbo pumps. The grounded chamber was pumped down to a base pressure of 10^{-7} Torr each time before the detection of target gases and subsequently purged with N_2 for 5 min to expel background gases and any water molecules adsorbed in the vacuum chamber. Next, target gases were introduced into the chamber through MFCs until equilibrium pressure was reached.

Electrical feedthrough with Triax to BNC adaptors enables the series connection of two source measure units (SMUs) of an HP4155 semiconductor parameter analyzer to gas detector electrodes. The connection of SMUs in series enabled us to record the current of each electrode separately. Measurements were conducted in room temperature and the applied voltage was in staircase sweep mode scanned in the range of 0-200 V ($\Delta V=1$ and $\Delta t=50$ ms). Guarded Triax cables were preferred to eliminate the capacitive leakage current. During the current-voltage measurement for each target gas, constant pressure was maintained through the proportional-integral-derivative (PID) controller.

2. Synthesis of patterned Si nanowires by using electroless etching technique: For the fabrication of one-dimensional (1-D) and two-dimensional (2-D) silicon structures using electroless etching (EE) technique, a patterned silver (Ag) thin film (20 nm) was coated on a pre-cleaned Si wafer using thermal evaporation technique. Next, it was immersed into two different solutions for selective etching, hydrofluoric-acid (HF)/silver-nitrate ($AgNO_3$) and HF/hydrogen-peroxide (H_2O_2). Results have shown that patterned Ag layer protects the underside of Si in HF/$AgNO_3$, while it catalyses in the HF/H_2O_2 solution. As can be seen in **Figure S1,** 1-D and 2-D Si structures, such as pillars, holes, walls and multiple geometrical shapes could be fabricated as long as patterned metal (Ag) layer is transferred onto the Si wafer before the EE process.

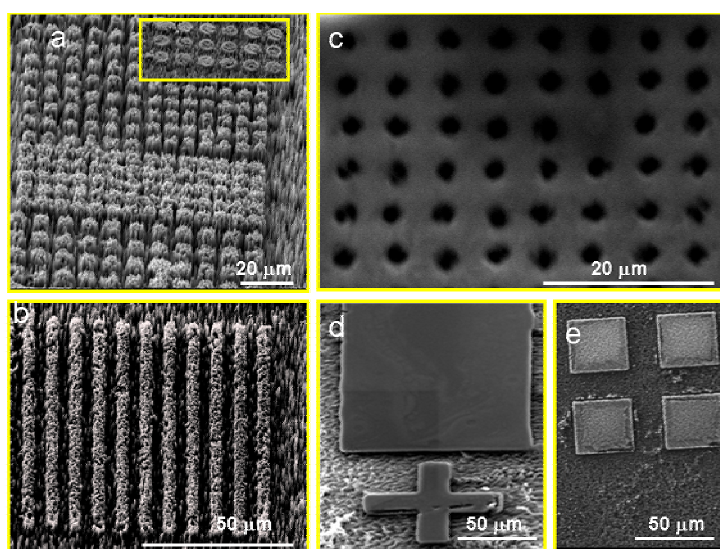

Figure S1. SEM images of fabricated (a) Si-pillars, (b) Si-walls, and (c) Si-holes in HF/$AgNO_3$ solution. (d-e) Different geometrical Si shapes fabricated in HF/H_2O_2.

3. Gas Discharging Mechanisms: A typical dark gas discharging mechanism is based on the generation of electron-ion pairs between two electrodes by the ionization of target gases through the interaction of neutral atoms or molecules with cosmic rays or natural radioactivity. Following the generation of electron-ion pairs (EIPs), they are accelerated in opposite directions in the presence of an applied field between two electrodes, and are

collected by the anode and cathode, respectively which then induces a small current in the external circuit[11]. The I-V curve of such discharge mechanism generally reveals four different regions in each of which current exhibits different electric field dependency[13, 14]. As shown in **Figure S2**, at low voltage (region 1), there is a nearly linear variation in current density (J) with applied electric field (E), which is given by

$$J=(n_e\mu_e+n_i\mu_i)eE \tag{S1}$$

where n_e and n_i are electron and ion concentrations, respectively; and, μ_e, μ_i are the mobilities of electrons and ions, respectively. In general, the I-V behavior in region 1 is determined by the field dependence of mobility and concentration of generated electron-ion pairs. This region is followed by region 2 in which the rate of increase in generated current with applied field decreases as a consequence of the increase in recombination rate of generated electron-ion pairs.

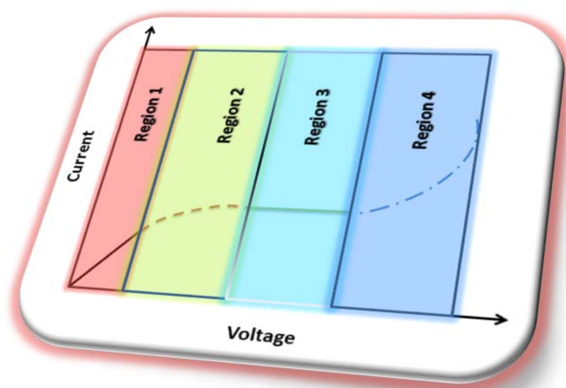

Figure S2. A typical current-voltage characteristic showing electrical discharges in gases.

In region 3, there is almost no field dependence of current density, called saturation current density, due to the equivalence in the rate of generation and collection of electron-ion pairs. Finally, in region 4, there is a remarkable increase in current with applied electric field, which is attributed to the generation of more EIPs by electron-impact process. Region 4 ends with breakdown voltage onset known as Townsend discharge, which was discussed in detail previously [33].

Based on analyses of I-V curves obtained for NH_3 and O_2 gases, it was found that both exhibit the typical behavior explained for the region 1 and 2 of a typical gas discharging mechanism, as shown in **Figure S3**.

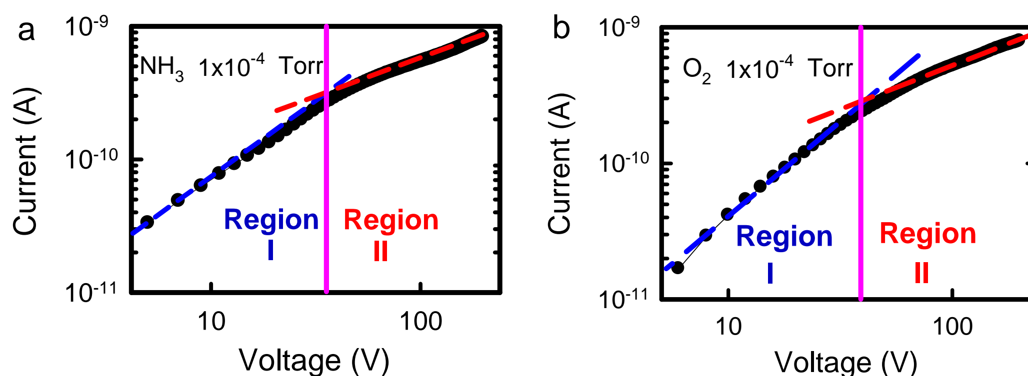

Figure S3. The I-V characteristics in log-log scale at gas pressure of 1x10^{-4} Torr for (a) NH_3 and (b) O_2 gases, respectively. Graphs reveal that the region I and region II, defined for a typical gas discharging gas sensor, appeared explicitly. The other regions, region 3 and 4, were not observed, which is probably stemming from the applied insufficient voltage in the studied range, which was constrained by our instrument's power limit during the measurement.

As it is summarized in **Table S1**, for NH_3, the current increases at first with increasing pressure up to a specific value (1x10^{-2} Torr at both 10 V and 100 V) and then starts to decrease with further increase beyond this value. The same trend is also valid for the O_2 except the shifting of maximum current from 1x10^{-2} Torr to 1x10^{-3} Torr at 100 V. The observed increase in current with increased pressure level below a critical value can be attributed to the dependence of generated current on the concentration of neutral gas molecules supplying EIPs via ionizing collisions that takes place between electron and neutral gas atoms or molecules. However, when the pressure is raised beyond this value, the mean free path of the generated charged particles (EIPs) decreases. This starts to dominate the field dependent behavior of current. At the high pressure region, the observed decrease in current with increasing gas pressure is reasonable as the short mean-free path of generated EHP recombinations decreases the probability of occurrence of more ionizing collisions between

ionized particles and neutral gas atom or molecules. In such a situation, the current is not determined predominantly by gas concentration any more, rather by mean free path of the charge carriers, particularly of electrons, which becomes the major parameter determining the kinetic energy of the free charges and their collection efficiency by electrodes. It is also very important to note that over the whole range of studied pressures (from $1x10^{-1}$ Torr to $1x10^{-5}$ Torr), when the measured currents for both gases are compared at a certain voltage, it is seen that there is a fluctuation in maximum current and it is exchanged between NH_3 and O_2 under different pressures.

Table S1. Measured currents at different pressures for NH_3 and O_2 gases

	10 Volt		100 Volt	
Pressure (Torr)	I_{NH3} (A)	I_{O2} (A)	I_{NH3} (A)	I_{O2} (A)
$1x10^{-1}$	$9.00x10^{-13}$	$2.90x10^{-12}$	$3.58x10^{-12}$	$2.38x10^{-12}$
$1x10^{-2}$	$1.61x10^{-10}$	$1.57x10^{-10}$	$6.07x10^{-10}$	$6.07x10^{-10}$
$1x10^{-3}$	$1.23x10^{-10}$	$1.41x10^{-10}$	$5.93x10^{-10}$	$7.08x10^{-10}$
$1x10^{-4}$	$4.16x10^{-11}$	$7.01x10^{-11}$	$5.40x10^{-10}$	$5.18x10^{-10}$
$1x10^{-5}$	$2.60x10^{-11}$	$4.58x10^{-11}$	$3.54x10^{-10}$	$4.08x10^{-10}$

For instance, within the pressure range of $1x10^{-5}$-$1x10^{-3}$ Torr at 10 V, the measured current for O_2 is higher than that obtained for NH_3, while it is lower than that obtained for NH_3 within $1x10^{-2}$-$1x10^{-1}$ Torr under same voltage bias. The difficulty in comparing the current obtained for different gases, based on a typical gas discharging mechanism, can be attributed to the presence of multi-parameters that can influence the discharging current, including the existence of large difference between the electronegativity of determined gases, their field dependent mobilities, different molecule weights, different type of electron-ion pair - space charge region interactions, and the absence of exactly the same physical condition during the testing of each gases (such as humidity, etc.).

3. Surface states induced by decoration of Si nanowires with a thin layer of Au: Based on the considerations of reported studies on introducing surface states to silicon by the deposition of a thin layer of Au[1717, 18, 19, 26], it is reasonable to expect the formation of the same states at the surface of Si NWs subsequent to the coating of 3 nm Au layer (see **Figure S4**), as is done in the present study.

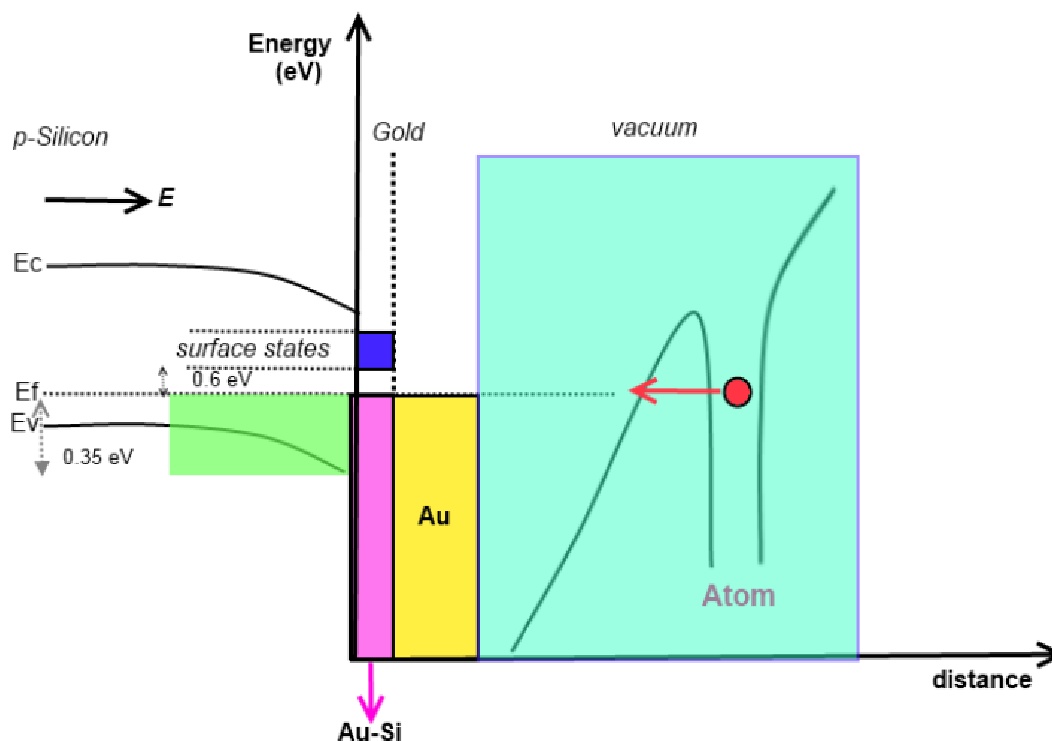

Figure S4. Schematic representation of field ionization near a Si tip doped with Au. The illustration shows the surface states at Au/Si interface formed following the decoration of Si NW with a thin layer of Au.

4. Detection of gases by FIGS Designed with Al coated Si NWs: We characterized Al doped Si NWs by fabricating sensors for detecting both NH_3 and O_2 gases. **Figure S5a** and **S5b** show the current (I)-voltage (V) characteristics measured in the pressure range of 10^{-2}-10^{-5} Torr and voltage range of 0-200 V for NH_3 and O_2 gases, respectively. It is clear from the graphs that in all the measured pressure ranges, devices show a typical gas discharge behavior for both gases, generally observed in the conventional planer gas sensors under uniform electric field, which is discussed in section 3 (gas discharging mechanisms). In other words,

the FI process based on quantum tunneling is not observed for the anodes designed with Al thin film (3nm) decorated NWs. These observations highlight the importance of Au induced surface states for the field ionization mechanism and verification of previous results suggesting the generation of surface states following the decoration of silicon with a thin layer of Au.

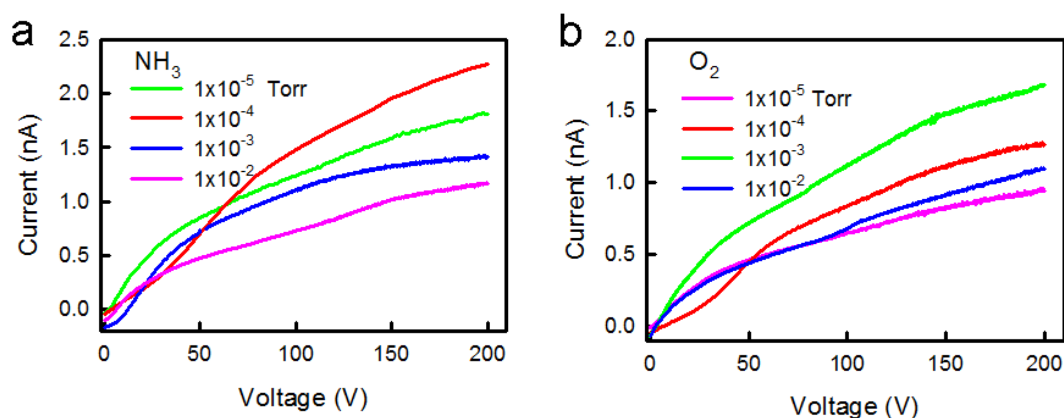

Figure S5. Current (I)-Voltage (V) characteristics of the FIGS based on Al doped Si NWs in the pressure ranges of $1x10^{-2}$-$1x10^{-5}$ Torr for (a) NH_3 and (b) O_2 gases. The FI process based on quantum tunneling is not observed for these anodes designed with Al thin film (3nm) decorated Si NWs.

[1] S. Kim, *Sensors* **2006**, 6, 503..
[2] R. Banan-Sadeghian, M. S. Islam, *Proc. SPIE* **2010**, 7679, 76791D.
[3] R. B. Sadeghian, M. Kahrizi, *Ieee Sens. J* **2008**, 8, 161.
[4] R. B. Sadeghian, M. Kahrizi, *Sensor Actuat a-Phys.* **2007**, 137, 248.
[5] H. F. F. Salvan, A. Baratoff and G. Binnig, *Surface Sci.* **1985**, 162, 634.
[6] L. B. Freeman, W. E. Dahlke, *Solid-State Electronics* **1970**, 13, 1483.
[7] P. Muret, A. Deneuville, *J Appl Phys* **1982**, 53, 6289.
[8] W. A. Schmidt, A. J. Melmed, M. F. Lovisa, M. Naschitzi, J. H. Block, *Surface Sci.* **1988**, 194, 127.
[9] S. M. Sze, *Cc/Eng Tech. Appl. Sci.* **1982**, 27, 28.